HHS Public Access

Author manuscript

Nat Cell Biol. Author manuscript; available in PMC 2020 January 29.

Published in final edited form as:

Nat Cell Biol. 2019 August ; 21(8): 940–951. doi:10.1038/s41556-019-0356-8.

The AMPK-Parkin axis negatively regulates necroptosis and tumorigenesis by inhibiting the necrosome

Seung Baek Lee[1,15], **Jung Jin Kim**[1,15], **Sang-Ah Han**[2], **Yingfang Fan**[3], **Li-Sha Guo**[4], **Khaled Aziz**[5], **Somaira Nowsheen**[5], **Sung Sun Kim**[6], **Seon-Young Park**[7], **Qifeng Luo**[8], **Jin Ook Chung**[7], **Sung Il Choi**[3], **Asef Aziz**[9,10], **Ping Yin**[1], **Seo-Yun Tong**[11], **Fabienne C. Fiesel**[12,13], **Wolfdieter Springer**[12,13], **Jin-San Zhang**[1,4,14,*], **Zhenkun Lou**[1,*]

[1]Division of Oncology Research, Mayo Clinic, Rochester, Minnesota, USA.

[2]Department of Surgery, School of Medicine, Kyung Hee University, Seoul, Republic of Korea.

[3]Department of Hepatobiliary Surgery, Zhujiang Hospital of the Southern Medical University, Guangzhou, Guangdong province, China.

[4]School of Pharmaceutical Sciences, Wenzhou Medical University, Zhejiang, China.

[5]Mayo Clinic Medical Scientist Training Program, Mayo Clinic Alix School of Medicine and Mayo Clinic Graduate School of Biomedical Sciences, Mayo Clinic, Rochester, Minnesota, USA.

[6]Department of Pathology, Chonnam National University Medical School, Gwangju, Republic of Korea.

[7]Department of internal medicine, Chonnam National University Medical School, Gwangju, Republic of Korea.

[8]Department of General Surgery, Shanghai Tenth People's Hospital, Tongji University School of Medicine, Shanghai 200072, P. R. China.

[9]Department of Pediatrics and Adolescent Medicine, Mayo Clinic, Rochester, Minnesota, USA.

[10]Saint Louis University School of Medicine, Saint Louis, Missouri, USA.

[11]Segaon Women's Hospital, Gangneung, Republic of Korea.

[12]Department of Neuroscience, Mayo Clinic, Jacksonville, Florida, USA.

[*]Correspondence zhang_jinsan@163.com (J.S.Z.), lou.zhenkun@mayo.edu (Z. L.).

Author contributions

S.B.L., J.J.K., and Z.L. designed, supervised, and performed most of the experiments, analyzed data, and prepared the manuscript as a lead author. S.B.L., J.J.K., A.A., K.A., and P.Y. performed animal experiments. F.C.F and W.S. provided the S65-ubiquitin homemade antibody. S.A.H, Y.F.F, S.S.K, S.Y.P, Q.F.L, J.O.C, S.I.C, S.N., A.A., K.A., and S.Y.T. helped with IHC analysis of human colon and inflammation-related small bowel tissue. S.N. participated in proofreading of this manuscript. J.S.Z participated in data analysis, technical assistance, manuscript writing and provided scientific insight and materials that made the study possible.

Competing interests

The authors declare no competing financial interests.

Additional information

Supplementary information is available in the Supplementary Materials.

Requests for materials should be addressed to Z.L (lou.zhenkun@mayo.edu).

[13]Neuroscience Program, Mayo Clinic Graduate School of Biomedical Sciences, Jacksonville, Florida, USA.

[14]The First Affiliated Hospital, Wenzhou Medical University, Wenzhou, Zhejiang, China.

[15]These authors contributed equally: Seung Baek Lee, Jung Jin Kim

Abstract

The receptor-interacting protein 1 (RIPK1)/RIPK3 kinases play important roles in necroptosis that is closely linked to inflammatory response. Although the activation of necroptosis is well characterized, how necroptosis is tuned down is largely unknown. Here, we found that Parkin (also known as *PARK2*), an E3 ubiquitin ligase implicated in Parkinson's disease and a tumor suppressor, regulates necroptosis and inflammation by regulating necrosome formation. Parkin prevents the formation of the RIPK1-RIPK3 complex by promoting polyubiquitination of RIPK3. Parkin is phosphorylated and activated by the cellular energy sensor AMP-activated protein kinase (AMPK). Parkin-deficiency potentiates the RIPK1-RIPK3 interaction, RIPK3 phosphorylation, and necroptosis. Importantly, Parkin deficiency enhances inflammation and inflammation-associated tumorigenesis. These findings demonstrate that the AMPK-Parkin axis negatively regulates necroptosis via inhibiting the RIPK1-RIPK3 complex formation and this regulation may serve as an important mechanism to fine-tune necroptosis and inflammation.

Introduction

The balance between pro- and anti-cell death signals is critical for tissue homeostasis and health of organisms[1–4]. Necroptosis is programmed necrosis or inflammatory cell death that links inflammatory response and tumor initiation and progression[5–12]. Receptor-interacting protein 3 (RIPK3) is the main initiator of necroptosis, and its phosphorylation promotes the formation of a functional complex called necrosome together with RIPK1[7, 11, 13–15]. Mixed lineage kinase domain-like (MLKL), the crucial mediator of necroptosis, is then activated at necrosome and triggers inflammatory reaction[11, 14]. However, how necrosome is negatively regulated remains largely unknown. Therefore, the study of the negative regulation of the necroptosis to maintain optimal immune response is of critical importance.

AMP-activated protein kinase (AMPK) is a highly conserved serine/threonine protein kinase that is activated under the conditions of depleted cellular ATP and elevated AMP levels, such as glucose deprivation[16, 17]. AMPK functions to monitor and maintain energy homeostasis. Previous studies including pre-clinical studies have also shown that AMPK has anti-inflammatory or anti-tumor functions. Interestingly, unlike other cell death signals, necroptosis is closely related to depletion of intracellular ATP. Therefore, there might be an unexplored link between AMPK and necroptosis.

Loss of Parkin's E3-ubiquitin ligase function is common in juvenile Parkinson's Disease (PD)[18–24] as well as in a variety of human cancers[25–30]. In the studies of inflammation in PD, *Parkin* knockout mice display increased susceptibility to inflammation-related degeneration[31]. *PARK2* heterozygosity also promotes colon cancer progression in mice with the mutant Adenomatous Polyposis Coli (APC) background[27]. However, how Parkin

functions as a tumor suppressor, especially the roles of Parkin in inflammation and cancer, is unclear. Here we found that the AMPK-Parkin axis is a critical regulator of necroptosis and inflammation, and dysregulation of this pathway contributes to inflammation-associated tumorigenesis.

Results

Parkin Knockout (KO) mice have increased inflammation

To study the physiological functions of Parkin, we used *Parkin* knockout (KO) mice. As shown in Figures 1a and 1b, *Parkin* KO mice at ten months of age showed multiple signs of inflammation and initial hyperplasia such as inflammatory infiltration in the small intestine, weight loss, increased the frequency of rectal prolapse (RP), elevated stool index (stool softness, blood in the stool) and splenomegaly. We hypothesized that increased inflammation due to *Parkin* deletion leads to tumor initiation or progression. To test our hypothesis, we assessed the levels of inflammatory markers TNF-α, IL-1β and IL-6 in the mouse small intestine and mouse embryonic fibroblasts (MEFs). Notably, the levels of these pro-inflammatory cytokines in the *Parkin* KO groups were significantly higher than those in the WT mice (Fig. 1c). 84 % (21 out of 25) of the *Parkin* KO mice had 5–10 intestinal polyps at 12 months of age, while none of the 25 WT mice developed polyps (Fig. 1d). To further investigate the relationship between Parkin and inflammation, we analyzed a cohort of ulcerative colitis samples (55 descending, 50 ascending colons) in the uninflamed or inflamed regions from clinically annotated gene-expression datasets[32] for Parkin expression (Fig. 1e). Within the cohorts, Parkin level was significantly lower in inflamed ascending or descending colon tissues compared to normal or uninflamed tissues. These results suggest that Parkin has an anti-inflammatory function.

Parkin negatively regulates necroptosis via inhibiting RIPK3 activation

Interestingly, we found increased necroptosis, but not apoptosis or autophagy, in *Parkin* KO MEFs or Parkin-knockdown HT-29 cells under T/C/Z or T/S/Z treatment [TNF-α (T) with Cycloheximide (C) or Smac mimetic (S) and the caspase inhibitor zVAD (Z)](Fig. 1f and Supplementary Fig. 1a). No increased sensitivity to necroptosis was observed in Parkin-knockdown cells under TNF-α alone or T/C treatment. No significant apoptotic event was observed under TNF-α or T/C/Z treatment (Supplementary Fig. 1b). We also found that RIPK1/RIPK3 and MLKL phosphorylation was elevated in tissues from *Parkin* KO mice, while no increase in caspase-3 cleavage, LC3-II, or TOM20 was observed (Fig. 1g). Knockdown of *Parkin* also increased RIPK3 and MLKL phosphorylation and necroptosis following T/C/Z or T/S/Z treatment in multiple cell lines (Supplementary Fig. 1c–f). Collectively, these data indicate that Parkin negatively regulates RIPK3 phosphorylation and thus TNF-α-induced necroptosis.

Parkin interacts with RIPK3 and negatively regulates RIPK1-RIPK3 interaction

We next examined the interaction between Parkin and pro-necroptotic factors, such as RIPK1 or RIPK3. Endogenous Parkin co-immunoprecipitated with RIPK3, but not RIPK1 or MLKL after T/C/Z treatment (Fig. 2a, b and Supplementary Fig. 2a, b). We also found that the IBR and R2 domains of Parkin were sufficient for RIPK3 interaction (Fig. 2c and

Supplementary Fig. 2c). However, IBR-R2 domain alone did not have any effect on necroptosis/RIPK3 activation (Fig. 2d). We next generated doxycycline-inducible expression vectors to express Parkin in *Parkin* KO MEFs. Interestingly, induction of Parkin resulted in decreased RIPK1-RIPK3 complex formation (Fig. 2e and Supplementary Fig. 2d). To further characterize the Parkin-RIPK3 interaction and identify the regions of RIPK3 that are required for its interaction with Parkin, we expressed FLAG-tagged RIPK3 deletion mutants and performed co-immunoprecipitation. The N-terminal domain of RIPK3 is required for its interaction with Parkin, whereas RIPK1 and RIPK3 interaction was mediated through the RHIM domain (Fig. 2f), suggesting that Parkin does not directly compete with RIPK1 for RIPK3 binding. Phosphorylation of RIPK1/RIPK3 is critical for the formation of a stable RIPK1-RIPK3 pro-necroptotic complex. In *Parkin* KO tissues, RIPK1/RIPK3 phosphorylation was increased (Fig. 1g), whereas Parkin overexpression inhibited RIPK3 phosphorylation and thus negatively controlling TNF-induced necroptosis in cells (Fig. 2g,h). Conversely, RIPK1 and RIPK3 protein interaction increased under necroptotic conditions in *Parkin* KO MEFs (Supplementary Fig. 2e, f). These results together suggest that Parkin inhibits the RIPK1-RIPK3 complex formation in response to necroptosis signals.

Parkin has been identified as a candidate tumor suppressor and is mutated in several human cancers[28, 29]. We hypothesized that mutations in Parkin might compromise its function in necroptosis and contribute to tumorigenesis. To test this hypothesis, we chose two human colon cancer-derived Parkin mutations, R420H[28], and H461R (http://www.cbioportal.org/). Both mutants affect residues locate within the IBR-R2 domain, which is the region that binds RIPK3 (Fig. 2c and Supplementary Fig. 2c). Interestingly, both mutations decreased Parkin interaction with RIPK3 (Fig. 2i) and failed to suppress RIPK3 phosphorylation or T/C/Z-induced necroptosis as opposed to the WT Parkin (Fig. 2j, k). Since we found that IBR-R2 domain alone is sufficient to mediate RIPK3 binding, but is unable to inhibit necroptosis/RIPK3 activation (Fig. 2c, d), we hypothesized that Parkin E3 ligase activity is required for the inhibition of RIPK3 activity. We, therefore, tested ubiquitin ligase deficient mutants (K161N and T240R Parkin). Interestingly, both mutant proteins were able to interact with RIPK3 similar to WT Parkin but were unable to suppress necroptosis (Fig. 2i). Thus, the E3 ligase activity of Parkin is necessary for its inhibition of necroptosis.

Parkin promotes RIPK3 polyubiquitination

We hypothesized that Parkin regulate polyubiquitination of RIPK3 following T/C/Z treatment. Indeed, we observed greatly reduced RIPK3 polyubiquitination in *Parkin* KO MEF cells (Fig. 3a). Moreover, overexpression of WT Parkin, but not its catalytically inactive mutant (C431S)[22–24, 29], increased polyubiquitination of RIPK3 (not RIPK1) under necroptotic conditions (Supplementary Fig. 4a). The activity of Parkin as a RIPK3 specific E3 ligase to promote RIPK3 ubiquitination *in vitro* was also validated (Supplementary Fig. 3a). However, overall RIPK3 protein level was not affected by Parkin expression (Supplementary Fig. 3b), suggesting that Parkin associates with RIPK3 and regulates its polyubiquitination, but not its stability. We further determined the linkage of Parkin-mediated ubiquitination of RIPK3 and discovered that Parkin mediates K33-linked polyubiquitination of RIPK3 (Fig. 3b–d). Significantly, we found that cancer-derived mutations (R420H and H461R) abolished the E3 ligase activity of Parkin (Fig. 3e). Previous

studies have shown that puncta-like RIPK3 subcellular localization is important for its function and is indicative of necrosome formation during necroptosis[14, 33]. We, therefore, tested the potential effect of Parkin on RIPK3's localization in cells undergoing necroptosis. As shown in Figures 3f and 3g, Parkin staining extensively overlapped with RIPK3, and mostly prevented its puncta distribution in response to T/C/Z observed in non-Parkin transfected cells. Furthermore, and R420H or H461R failed to prevent puncta-like localization of RIPK3 during necroptosis (Fig. 3f, g). T/C/Z treatment did not induce polyubiquitination of TOM20 and PLK1, two other reported Parkin substrates during mitophagy and mitosis, respectively (Supplementary Fig. 4a)[22–24, 29]. Conversely, treatment with carbonyl cyanide m-chlorophenylhydrazone (CCCP), a mitochondrial-uncoupling reagent that activates Parkin during mitophagy[22–24], induced TOM20 ubiquitination but not RIPK3 ubiquitination. CCCP treatment also failed to activate RIPK3 (Supplementary Fig. 4a–g). We next analyzed potential RIPK3 ubiquitination sites from mass spectrometry analysis (http://www.phosphosite.org). Among these, mutations of lysine (K) at K197, K302 or K364 sites to arginine (R) substantially reduced RIPK3 polyubiquitination (Fig. 4a). As shown in Figure 4b, mutating all three residues (3KR) largely abolished RIPK3 ubiquitination induced by T/C/Z. We, therefore, predicted that the 3KR mutants would be resistant to Parkin-mediated RIPK3 inhibition. Indeed, we found that Parkin induction decreased necroptosis, RIPK1-RIPK3 interaction, RIPK3 or MLKL phosphorylation, and RIPK3's punctuation in cells expressing WT RIPK3 but had no effect on cells expressing RIPK3 3KR mutant (Fig. 4c–g). Collectively, these data indicate that Parkin specifically promotes RIPK3 polyubiquitination under necroptotic conditions to negatively regulate necroptosis.

Parkin is phosphorylated at ser 9 by AMPK and activated during necroptosis

Previous studies suggest that Parkin phosphorylation, as well as ubiquitin (Ub) phosphorylation by PINK1, is necessary for full activation of Parkin's E3 ligase activity. However, we found that PINK1 did not contribute to Parkin activation for RIPK3 / necroptosis inhibition under necroptosis stimuli (Supplementary Fig. 4d, e). Next, we tested whether PINK1-dependent ubiquitin phosphorylation impacts Parkin activity during necroptosis. Interestingly, ubiquitin-S65 phosphorylation by PINK1 was not involved in Parkin activation during necroptosis (Supplementary Fig. 5a). Together, our data suggest that neither ubiquitin-S65 nor PINK1 is involved with Parkin activation during necroptosis.

We have previously observed in a separate project[34] that *AMPK* KO cells showed enhanced T/C/Z-induced cell death (Fig. 5a). Depletion of intracellular ATP is one of the main features of necroptosis[35, 36]. We found that RIPK3 is hyperactivated in *AMPK* KO cells following T/C/Z treatment, resembling our observation in *Parkin* KO cells (Fig. 5b and Supplementary Fig. 5b). Of note, RIPK3 and MLKL phosphorylation reached their peaks at 4 h after T/C/Z treatment and then started to decrease, whereas AMPK was found slightly phosphorylated at 2 h and but kept steadily increasing up to at least 8 h. Moreover, without RIPK1 or RIPK3, AMPK phosphorylation is prevented, suggesting AMPK activation under necroptosis is RIPK1/ and RIPK3 dependent (Supplementary Fig. 5c). Interestingly, AMPK phosphorylation was similar in control and MLKL-deficient cells until 4h post T/C/Z treatment. However, it significantly decreased at later time points in MLKL deficient cells

(Supplementary Fig. 5d). This suggests that the initial AMPK activation is RIPK dependent and MLKL activation or low ATP during necroptosis may be the main source of the sustained activation of AMPK. The serine 9 (S9) residue on Parkin is predicted to be an AMPK phosphorylation site (http://gps.biocuckoo.org/) and its surrounding sequence fits with a consensus AMPK phosphorylation motif, LXRXX(pS/pT) (Supplementary Fig. 5e,f)[34, 37]. Therefore, we hypothesized that Parkin is a substrate of AMPK. Using an antibody recognizing AMPK substrates, we confirmed that under necroptosis, Parkin is phosphorylated in *AMPK*-proficient cells, but not in *AMPK*-deficient cells (Fig. 5c). AMPK itself is also activated under necroptotic conditions (Fig. 5b and Supplementary Fig. 5g). Mutating S9 of Parkin to alanine (S9A) impaired not only AMPK phosphorylation, but also its inhibition of RIPK3 phosphorylation (Fig. 5d,e), suggesting that phosphorylation of this residue is crucial for Parkin's function in regulating RIPK3. We further confirmed that AMPK could directly phosphorylate Parkin S9 *in vitro* (Fig. 5f). Collectively, these results demonstrate that AMPK-mediated phosphorylation of Parkin is important for the regulation of the Parkin-RIPK3 pathway during necroptosis. It is worth mentioning that Parkin S9 is highly conserved among vertebrates (Supplementary Fig. 5f), suggesting that S9 phosphorylation may have an evolutionarily conserved role in regulating Parkin activity.

Parkin is inactive in unstressed cells. It is possible that the S9 phosphorylation, like the S65 phosphorylation during mitophagy, activates Parkin E3 ligase activity. To confirm the regulation of Parkin-RIPK3 pathway by AMPK, we examined RIPK3 ubiquitination, and observed that T/C/Z-induced RIPK3 ubiquitination was compromised in *AMPK* KO cells (Fig. 5g). Ubiquitination of RIPK3 was also abolished by the S9A mutation (Fig. 5h,i and Supplementary Fig. 5j). Conversely, the S9D mutation, which mimics S9 phosphorylation, dramatically enhanced RIPK3 ubiquitination (Fig. 5h,i and Supplementary Fig. 5h), consistent with enhanced Parkin E3 ligase activity. However, mutating PINK1 phosphorylation site on Parkin (S65A)[22–24, 29] did not affect necroptosis (Fig. 5d and Supplementary Fig. 5h). Expression of Parkin S9D mutant, but not WT or S9A, induced RIPK3 ubiquitination and inhibited necroptosis (Fig. 5i,j), suggesting that Parkin activation requires AMPK.

AMPK is activated by T/C/Z treatment, and its activation is independent of Parkin (Supplementary Fig. 5i). In addition, downregulation of Parkin in *AMPK* KO cells had no further effect on T/C/Z-induced necroptosis (Fig. 5i, j), suggesting that AMPK and Parkin are epistatic with regards to the regulation of necroptosis. Indeed, treatment with either metformin[38] or phenformin[37], which triggers metabolic stress and activates AMPK, inhibited RIPK3 and T/C/Z treatment-induced necroptosis in *Parkin*-proficient cells, but had no effect in *Parkin*-deficient cells (Supplementary Fig. 6a–f). We also found that T/C/Z induced RIPK3 and MLKL phosphorylation, as well as RIPK3 polyubiquitination, were drastically suppressed by metformin or A-769662, which are indirect and a direct AMPK activator (Supplementary Fig. 6g, h). In addition, we could confirm Parkin (S9) phosphorylation following A-769662 treatment (Supplementary Fig. 6i). However, AMPK activator alone did not have impact on RIPK3 phosphorylation and its polyubiquitination without necroptotic stimuli (Supplementary Fig. 6g and 6h). Collectively, these data indicate that AMPK-mediated phosphorylation of Parkin at S9 residue is another mode of Parkin activation important for its function in necroptosis.

The AMPK-Parkin axis suppresses intestinal inflammation and colitis-associated tumorigenesis in AOM/DSS mouse model

We have shown that *Parkin* ablation contributed to the development of polyps in the small intestine (Fig. 1d). As Parkin has other cellular functions, such as regulation of mitophagy, we wanted to address which function of Parkin is important for tumor suppression. We utilized N-(6-(Isopropylsulfonyl) quinolin-4-yl)benzo[d]thiazol-5-amine (GSK'872), a RIPK3 inhibitor[39, 40], to treat mice to determine whether misregulated necroptosis in *Parkin* KO mouse contributes to tumorigenesis. GSK'872-treated mice exhibited reduced RIPK3 phosphorylation and intestine polyps with increased survival (Fig. 6a–e), suggesting that hyperactivation of RIPK3 and necroptosis are important for tumorigenesis in *Parkin* KO mice. We confirmed that GSK'872 treatment significantly reduced punctation of RIPK3 as well as necroptosis without imposing discernible toxicity in normal mice by measuring body weight, alanine aminotransferase (ALT) and aspartate aminotransferase (AST) levels, as well as liver histopathological analysis (Supplementary Fig. 7a–e). Necroptosis is linked to inflammation[7, 11], and chronic inflammation is suggested to be a high-risk factor for colorectal cancers[8–10]. *Parkin* KO mice had higher expression of pro-inflammatory cytokines (Fig. 1c and 6e), while GSK'872 treatment reduced the expression of these cytokines (Fig. 6e), suggesting that hyper-inflammation in *Parkin* KO mice is due to RIPK3 hyperactivation. Inflammatory bowel disease is a salient example of the link between chronic inflammation and cancer[8–11]. We, therefore, used the AOM/DSS model of colitis (inflammation) associated cancer[5, 6] to further study the role of Parkin in the inflammation-related tumorigenesis (Fig. 6f–j). A shortened protocol was adopted to study whether Parkin deficiency accelerates polyp formation. Compared to WT mice, *Parkin*-deficient mice had increased RIPK3 phosphorylation, higher expression of pro-inflammatory cytokines, a higher number of polyps and decreased survival (Fig. 6f–j). GSK'872 treatment again drastically reduced AOM/DSS-induced RIPK3 phosphorylation, pro-inflammatory cytokine expression and polyp formation (Fig. 6f–i). Since RIPK3 has multiple pro-inflammatory effects independent of necroptosis, we next examined the effect of GW806742X, a MLKL inhibitor, on the AOM/DSS model. GW806742X treatment markedly reduced expression of pro-inflammatory cytokines and polyp formation in *Parkin* KO mice (Supplementary Fig. 7f). Taken together, our results suggest a protective role of Parkin against RIPK3-mediated necroptotic inflammation-induced tumorigenesis. Moreover, we found that AMPK activators, Metformin and A-769662, also dramatically suppress intestinal polyp growth in AOM/DSS WT mice but has little effect on *Parkin* KO mice (Fig. 7a–c and Supplementary Fig. 7g–i). AMPK is activated by metformin in polyps and areas of inflammation (Fig. 7c). Significantly, in *Parkin* KO mice, even though metformin could also activate AMPK, it did not suppress intestinal polyp growth. These data suggest that AMPK can suppress necroptosis and inflammation-related tumorigenesis by regulating Parkin activation.

Finally, we found a negative correlation between Parkin expression and phosphorylation of RIPK3 in 108 normal human colon tissue and colon cancer tissues and 412 human inflammatory bowel disease (IBD, Crohn's disease or Ulcerative colitis) patient specimens by immunohistochemical (IHC) staining (Fig. 7d–f). These results are consistent with the negative regulation of phosphorylation of RIPK3 by Parkin in human patient samples.

Discussion

Necroptosis is emerging as the significant cellular signal pathway in cancer. In this study, we propose that AMPK and Parkin cooperate to regulate necrosome activation, necroptosis, and necroptosis-induced inflammatory tumor formation. Our findings suggest AMPK is activated under necroptosis-inducing condition and phosphorylates/activates Parkin, which in turn negatively regulates necroptosis by promoting polyubiquitination (linkage-specific K33) of RIPK3 and suppression of necrosome formation. Loss of AMPK or Parkin increases the activation of RIPK3 and leads to increased necroptosis, which is a primary source of inflammation (Fig. 7g).

One surprising finding is that AMPK is activated under necroptotic conditions without any known stimulation such as starvation or deprivation of glucose. Intracellular ATP levels play a crucial role in the interchange between apoptosis and necrosis. Apoptosis, the energy-requiring cell death, is switched to necroptosis when intracellular ATP levels are depleted[41–44]. We showed that without RIPK1 or RIPK3, AMPK activation is prevented in necroptosis, suggesting AMPK is activated in a RIPK1 and RIPK3 dependent manner (Supplementary Fig. 5c). However, AMPK phosphorylation keeps increasing even when RIPK1/3 phosphorylation has started to decline (Supplementary Fig. 5c). Interestingly, in MLKL deficient cells, we did not detect any difference in AMPK phosphorylation until later time points (Supplementary Fig. 5d). Given that activated AMPK, in turn, phosphorylates Parkin to activate Parkin's E3 ligase function, it is possible that the initial AMPK activation is RIPK1 or RIPK3-dependent and then low ATP during necroptosis may serve as the second activator of AMPK. We suggest that sustained activation of AMPK by RIPK1/RIPK3/MLKL may serve as a negative feedback mechanism to restrain overt necroptosis through Parkin, therefore contributing to maintaining cellular homeostasis including optimal immune response. It will be interesting to dissect how AMPK activation is initiated and sustained in greater detail in future studies.

It has been previously reported that PINK1-dependent Parkin phosphorylation (S65) within the Ubl domain activates Parkin E3 ligase activity by inducing a conformational change. Interestingly, AMPK also phosphorylates Parkin at S9 at the N-terminal Ubl domain. This might suggest an activation mechanism of Parkin in which initial phosphorylation at S9 by AMPK leads to disruption of the interaction between the Ubl domain and C-terminus of Parkin. It has been previously reported that PINK1-induced phosphorylation of ubiquitin at S65 plays a critical role in mediating Parkin activation,[24] However, neither ubiquitin-S65 phosphorylation nor PINK1 was involved in Parkin activation during necroptosis (Supplementary Fig 4d, e, 5a). Future studies are needed to determine whether ubiquitin itself is modified during necroptosis for Parkin activation.

In conclusion, we suggest that AMPK/Parkin/RIPK3 pathway is a key regulatory mechanism of necroptosis and inflammation-induced tumorigenesis. Our discovery also explains how Parkin loss or mutation contributes to human colon cancer development and therefore reveals a potential target for the therapeutic invention to treat or prevent human colorectal cancer.

Methods

Mouse strains and MEFs

All animal procedures were approved by the Institutional Animal Care and Use Committee. Mouse strains were described previously[29]. *Parkin* KO C57BL/6 (6–8 weeks old, female) mice were purchased from the Jackson Laboratory (Bar Harbor, ME, USA) and mated. Animals were housed in a pathogen-free barrier environment throughout the study. Mouse embryonic fibroblasts (MEFs) were isolated from embryonic day 11.5–13.5 (E11.5-E13.5) by uterine dissection for individual embryos. Each embryo was washed softly with 1x PBS (pH 7.2), followed by removal of the mouse embryo's head and liver. The embryo body was suspended in 0.5 ml of 0.25% Trypsin-EDTA, and then forced through a 1 ml syringe with an 18-gauge needle. The tissue homogenate was incubated for 30 min at 37°C, triturated by drawing the suspension through a pipette, and then evenly-divided into two 10 cm tissue culture dishes in Dulbecco's modified Eagle's medium (DMEM) with 15% fetal bovine serum (FBS). Immortalized MEFs were used for all experiments, and at least three lines were examined for all studies. *AMPK* KO MEFs, which are deleted of the AMPK alpha1 and alpha 2 genes, were described previously[34].

Cell Culture and reagents

All cell lines were purchased from commercial vendors. *Parkin* and *AMPK* KO and WT MEFs were cultured in Dulbecco's modified Eagle's media (DMEM, Gibco-Invitrogen). Three human colon adenocarcinoma cell lines, HT-29, COLO205, and HCT116, human embryonic kidney (HEK) 293T cells, human bone osteosarcoma U2OS and human epitheloid cervix carcinoma HeLa were obtained from the American Type Culture Collection (ATCC, Manassas, VA). Cells were cultured in DMEM containing 10% heat-inactivated FBS (Gibco-Invitrogen), sodium bicarbonate (2 mg/ml; Sigma-Aldrich, St Louis, MO), penicillin (100 units/ml), and streptomycin (100 μg/ml; Gibco-Invitrogen). TNF-α, Cycloheximide, and the caspase inhibitor zVAD (V116), carbonyl cyanide m-chlorophenylhydrazone (CCCP; a mitochondrial uncoupler and a chemical inhibitor of oxidative phosphorylation, C2759), Metformin (PHR1064), Phenformin (water-soluble phosphorylate AMP-activated protein kinase (AMPK) activators), GW806742X (SML1990) and Azoxymethane (AOM, A5486) were purchased from Sigma-Aldrich. Dextran Sulfate Sodium (DSS, 0216011090) was purchased from MP Biomedicals. N-(6-(Isopropylsulfonyl)quinolin-4-yl)benzo[d]thiazol-5-amine [GSK'872; RIPK3 (receptor-interacting protein kinase-3) inhibitor (530389)] was purchased from Calbiochem. Smac mimetic (AEG 40730 dihydrochloride) and A-769662, AMP-activated protein kinase (AMPK) activator, was purchased from Tocris.

Plasmids

HA, GFP or Flag-tagged Parkin plasmids (empty and WT, Ubl deletion, Ubl, Linker only, R1-IBR, IBR-R2, IBR, R1 and R2 only) were kindly provided by Dr. Jennifer L. B. Roshek, Dr. Darren J. Moore, Dr. Ted M. Dawson (The Johns Hopkins University School of Medicine, Baltimore, Maryland), Dr. Erkang Fei and Dr. Guanghui Wang (University of Science & Technology of China, China). These constructs have been described previously[20,21]. HA-tagged Parkin plasmids (empty and WT, S65A, S65D, S378A, S378D,

C431A, and C431S) were kindly provided by Dr. Noriyuki Matsuda (Tokyo Metropolitan Institute of Medical Science, Tokyo, Japan) and have been described previously[22]. Myc-tagged Parkin constructs (empty and WT, S9A, S9D, S101A, S131A, S136A, S296A, S378A, S384A and S407A) were kindly provided by Dr. Christian Haass (Laboratory of Alzheimer's and Parkinson's Disease Research, Department of Metabolic Biochemistry, Ludwig Maximilians University, Germany)[19] and some of the mutants were generated by site-directed mutagenesis. The doxycycline-inducible Parkin construct, pcDNA6/TR-Parkin, was kindly provided by Dr. Nadja Patenge (Center of Neurology and Hertie Institute for Clinical Brain Research, Tübingen, Germany) and was described previously[45]. HA-tagged ubiquitin and ubiquitin lysine mutants, such as K-6 only, K-11 only, K-27 only, K-29 only, K-33 only, K-48 only, K-63 only, K33R, K48R, and K63R were obtained from Addgene. The human Flag-RIPK3 constructs (WT, tetra-Ala RHIM domain (amino acids 459–462) substitution (mutRHIM), K50A, S227A, and K50A plus tetra-Ala RHIM domain substitution (K50mutRHIM), K42R, K55R, K62R, K197R, K302R, K364R, K501R, and 3KR) constructs were kindly provided by Dr. Edward S. Mocarski (Emory University School of Medicine) as described previously[46] or were generated by site-directed mutagenesis. Flag-tagged and HA-tagged- mouse RIPK3 vectors [Flag, WT and mutants, such as AAAA (mut-RHIM), K51A, D143N, T231A/S232A (kinase inactive mutants)] constructs were kindly provided by Drs. Francis Ka-Ming Chan and Sakthi Balaji (University of Massachusetts Medical School). The constitutively active GST-AMPK kinase domain (GST-AMPK-CAD, T172D) was kindly provided by Dr. Yick-Pang Ching (The University of Hong Kong, China).

Primers and real-time RT-PCR

RNA preparation, cDNA, and qRT-PCR were described previously[30]. The following primers were used for Real-Time PCR (qRT-PCR).

TNF-α Primer sequence:

Forward 5'-CCAGCCAGCAGAAGCTCCCTCAGCGAG-3',

Reverse5'-GCGGATCATGCTTTCTGTGCTCATGGTGTC-3'

IL-6 Primer sequence:

Forward 5'-CCTGCGTTTAAATAACATCAGCTTTAGCTT-3',

Reverse 5'-GCACAATGTGACGTCGTTTAGCATCGAA-3',

IL-1β Primer sequence:

Forward 5'-CACAGCAGCACATCAACAAG-3',

Reverse 5'-GTGCTCATGTCCTCATCCTG-3',

Gene silencing by shRNAs, transfection and lentivirus infection

Parkin and *PINK1* shRNAs were obtained from Sigma-Aldrich and Open Biosystems.

Parkin shRNA (Open Bio.)

Company Species Clone Set ID Names Target sequence (5’- −3’)

Open Bio. Human NM_013988 84517 5’-GAGAGAGTTCTCACATTTAAT-3’

Open Bio. Human NM_013988 84518 5’-ACTCACTAGAATATTCCTTAT −3’

Open Bio. Human NM_013988 84520 5’-GAACGTTTAGAAATGATTTCAAA −3’

Parkin shRNA (Sigma)

Company Species Clone Set ID Names Target sequence (5’- −3’)

Sigma (TRC1) Human NM_013988 2399 5’-CGTGAACATAACTGAGGGCAT-3’

Sigma (TRC1) Human NM_013988 341 5’-CGCAACAAATAGTCGGAACAT-3’

Sigma (TRC1) Human NM_013988 425 5’-CGTGATTTGCTTAGACTGTTT-3’

Sigma (TRC1) Human NM_013988 434 5’-CTTAGACTGTTTCCACTTATA-3’

Sigma (TRC1) Human NM_013988 872 5’-CTCCAAAGAAACCATCAAGAA-3’

PINK1 shRNA

Company Species Clone Set ID Names Target sequence (5’- −3’)

Open Bio. Human NM_032409 234804

5’-CGTATGTGCCTTGAACTGAATTAGTGAAGCCACAGATGTAATTCAGTTCAAGG

CACATACGT-3’

Open Bio. Human NM_032409 235108

5’-GGGAGCCATCGCCTATGAAATTAGTGAAGCCACAGATGTAATTTCATAGGCG

ATGGCTCCCA-3’

Open Bio. Human NM_032409 238759

5’-GCCGCAAATGTGCTTCATCTATAGTGAAGCCACAGATGTATAGATGAAGCACA

TTTGCGGCT-3’

Co-immunoprecipitation, immunoblotting, and antibodies

For immunoprecipitation, extraction of proteins with a modified buffer from cultured cells was followed by immunoprecipitation and immunoblotting with corresponding antibodies. Rabbit polyclonal antibodies recognizing PINK1 (ab23707), RIPK3 (ab152130, ab56164) and LC3 I/II (ab51520) were obtained from Abcam. Mouse monoclonal antibodies

recognizing RIPK1 (ab72139) and phospho-RIPK3 (ab205421, ab209384) were purchased from Abcam. Rabbit polyclonal antibody recognizing Tom20 (sc-11415), MLKL (sc-293201), mouse monoclonal antibody recognizing Parkin (sc-32282) and RIPK3 (sc-374639) were purchased from Santa Cruz Biotechnology. Mouse monoclonal antibodies recognizing Parkin (#4211) was obtained from Cell Signaling. Rabbit polyclonal antibodies recognizing Parkin (#2132), phospho-RIPK3 (#57220) and phospho-MLKL (#91689), phospho-AMPK (#2531), Caspase-3 (#9662), phospho-RIPK1 (#65746), Phospho-Ubiquitin (Ser65) (#37642) and Phospho-AMPK Substrate Motif [LXRXX(pS/pT), #5759] were also purchased from Cell Signaling. Mouse monoclonal antibody recognizing Plk1 was obtained from Invitrogen. RIPK3 (R4277), Myc, FLAG (m2), and HA mouse antibodies were purchased from Sigma. Light-chain-specific anti-mouse and anti-rabbit IgG secondary antibodies were obtained from Jackson Immunoresearch. pS65-ubiquitin (#3149 ID6–9N) were kindly provided by Dr. Wolfdieter Springer (Mayo Clinic, Jacksonville, Florida).

Doxycycline-inducible Parkin tet-on system cell lines

The pcDNA6/TR (Flag or Myc)-Parkin was kindly provided by Dr. Nadja Patenge[7]. Subconfluent 1×10^6 HT-29 or *Parkin* KO cells were transfected with the pTet-On plasmid using Lipofectamine™ 2000 (Invitrogen, Carlsbad, CA). At 24 h after transfection, the medium was removed and cells were washed with 1x PBS at 37 °C, and then supplemented with complete media containing 300 mg/ml of zeocin (Invitrogen) for selection of positive Parkin clones. Parkin expression was induced by the addition of 1–2 mg/ml doxycycline (Sigma) for 24 h to the culture medium.

Expression and purification of the recombinant protein

HA or GFP-tagged Parkin from Dr. Noriyuki Matsuda (Tokyo Metropolitan Institute of Medical Science, Tokyo, Japan) was cloned into pGEX-4T-1 (Amersham Pharmacia Biotech, Piscataway, NJ) vector using EcoRI/NotI restriction enzyme sites as previously described[6]. BL21 E. coli (Life Technologies) was transformed with the pGEX-4T-1 (GST-only and Parkin WT) vectors. Positive E. coli BL21 colonies containing pGEX-4T-1/Parkin were cultured in 3–5 ml Luria-Bertani (LB) medium (with ampicillin) at 37°C overnight, after which the culture was transferred to fresh 600 ml LB liquid medium (with ampicillin) for 2–3 h. When the optical density reached a wavelength of 400–600 nm, isopropyl β-D-1-thiogalactopranoside (IPTG) was added with a final concentration of 0.4 M, and the culture was shaken at 18°C overnight. The bacteria were then collected, and sonicated on ice in 1x NETN buffer supplemented with complete protease inhibitor, aprotinin. After centrifugation at 5,000 × g for 10 min at 4°C, the supernatant was purified using a glutathione S-transferase (GST) purification resin column (Novagen; Merck KGaA, Darmstadt, Germany) including aprotinin and PMSF by rocking at 4°C for 18 h. After washing six times with 1xNETN, GST-Parkin was eluted with GSH elution buffer (30 mM reduced glutathione, 1 % Triton X-100, 500 mM Tris-HCl, pH 8.8). The integrity and yield of purified His-tagged fusion proteins as well as commercial RIPK3 recombinant proteins (Novus Biologicals, H00011035-P01) were assessed by SDS PAGE followed by Coomassie blue staining. All His-tagged recombinant proteins were purified using TALON resin (CLONTECH) according to the manufacturer's protocol with minor modifications. Beads were washed three times with 10 ml of PBS buffer (200 mM washing buffer). Proteins were eluted with

300–500 ml of elution buffer (same as binding buffer except with 100 mM imidazole). Eluted proteins were concentrated to 1–2 mg per ml using a microconcentrator (Filtron). Protein samples were fractionated on 10% SDS polyacrylamide gels and stained by Coomassie brilliant blue G250.

in vivo and *in vitro* ubiquitination assays

For *in vivo* ubiquitination, cells were transfected with His-tagged ubiquitin plasmid together with HA or HA-Parkin (WT, C431S, R420H or H461R) constructs. Cells were treated with T/C/Z; TNF-α (20 ng/mL), CHX (10 μg/mL) and z-VAD (20 μM) or CCCP (10 μM). 48 h post-transfection, cells were lysed by Urea lysis buffer (8 M Urea, 0.1 M Na_2HPO_4, 0.1 M Tris / HCl (pH 8.0), 0.05% Tween 20 and 0.01 M imidazole). After centrifugation, the supernatants were collected and incubated with 20 ml Ni-NTA agarose beads (Qiagen) for 4 hours at 4°C. The precipitates were washed three times with Urea wash buffer (8 M Urea, 0.1 M Na_2HPO_4, 0.1 M Tris / HCl (pH 8.0), 0.05% Tween 20 and 0.02 M imidazole) and Native wash buffer (0.1 M Na_2HPO_4, 0.1 M Tris / HCl (pH 8.0), 0.05% Tween 20 and 0.02 M imidazole). Samples were boiled with SDS loading buffer and then subjected to SDS-PAGE followed by immunoblot analysis. *In vitro* ubiquitination assay was performed in 30μl of ubiquitination reaction buffer (50mM Tris·HCl pH 7.5, 2mM $MgCl_2$, 2mM ATP, 10μg/μL Myc-ubiquitin) with 50ng of E1 (Ube1; Boston Biochem), 200ng of E2 (UbcH7; Boston Biochem), 2 μg of E3 (purified Parkin, Wt, S65A, S65D, S378A or S378D), and 10ng of substrate (RIPK3, Abnova). Parkin and RIPK3 were cloned into pGEX-2TK, pGEX-4T-1 or pRSETA vectors and the expressed proteins were purified. The reaction was performed for 90 min at 30 °C. Equal volumes of each sample were prepared for immunoblot. The reaction products were analyzed by immunoblotting with ubiquitin antibody.

in vitro kinase assays

Kinase assay has been described previously[1]. GST-AMPK catalytic domain T172D (GST-AMPK-CAD) was incubated with wild-type or Ser 9A mutant of GST-Parkin recombinant (molar ratio 1:50) in 10 μl AMPK kinase buffer in the presence of 10 μCi -[γ–^{32}P] ATP at 30°C for 1 h. Incorporation of [^{32}P]ATP into substrates was detected by autoradiography. AMPK and Parkin were also detected by immunoblotting using anti-AMPK and anti-Parkin antibodies, respectively.

Immunofluorescence microscopy for PI staining

For immunofluorescence staining, HT-29, COLO205, HCT116, *Parkin* WT and KO, and *AMPK* WT and KO MEFs were plated on glass coverslips and transfected with the indicated constructs. Cells were stained with PI, fixed in 3.7 % paraformaldehyde for 10 min at room temperature and stained using standard protocols. Immunofluorescence images were taken using fluorescent microscope (Nikon Microscope, Melville, New York).

AOM/DSS-induced colitis-associated colon cancer mice model

In AOM/DSS-induced colitis-associated colon cancer model, we set aside cages of sex and age matched (6–8 week)-old C57BL/6 mice to be used for experimental and control groups. On day 0, mice were given a single peritoneal injection (intraperitoneally, IP) of AOM (10

mg/kg) working solution (1 mg/ml in isotonic saline, diluted from 10 mg/ml stock solution in H_2O kept at −20 °C). Seven days later, 2.0 % DSS solution (2.0 g/100 ml) was administered for 5 days followed by free water consumption for 16 days. This cycle was repeated two (for Fig. 6f–j) or three times (for Fig. 7a–c). *Parkin WT* and *KO* mice (*n=15*) were treated to establish an AOM/DSS model of colitis-associated colon cancer (CAC). These mice were then treated intravenously (i.v.) with the vehicle control or 1.0 mg/kg GSK'872 twice weekly for 7–8 weeks, or were fed metformin (300 mg/kg) for 10 weeks. Body weight, incidence of rectal prolapse (RP), stool index (blood content in the stool), and survival was measured every week. The mice were euthanized 10 days after the last 2.0 % DSS administration. After euthanization, number of polyps, levels of cytokines (TNF-α, IL-1β and IL-6) and phospho-RIPK3 were measured. To check the toxicity of GSK'872, we assessed the body weight, alanine aminotransferase (ALT) and aspartate aminotransferase (AST) levels, and performed liver histopathological analysis.

Immunohistochemistry

The paraffin sections of human colon cancer tissues and human inflammatory bowel disease patient were obtained from the tissue repository at Kyung Hee University Medical School, Chonnam National University Medical School (South Korea), and Zhujiang Hospital of the Southern Medical University (China) with approval from each of the hospital's internal committees for human tissue uses. We affirm that the study is compliant with all relevant ethical regulations regarding research involving existing specimens with informed consent obtained from all participants. IHC was performed following standard protocol. Briefly, immunohistochemical cytokeratin staining was performed on formalin-fixed, paraffin embedded tissue using an indirect immunoperoxidase technique. Sections mounted on slides were dewaxed in xylene, dehydrated in ethanol, boiled in 0.01 M citrate buffer (pH 6.0) for 20 min. in a microwave oven and then incubated with 3 % hydrogen peroxide for 5 min. After washing with PBS, the slides were incubated in 10 % normal BSA for 5 min, followed by incubation for 45 min with rabbit polyclonal antibodies recognizing Parkin (ab15954, 1:200) and mouse monoclonal antibody recognizing anti-phospho-RIPK3 (Abcam, ab205421, 1:200). After washing, sections were incubated with labeled polymer (Bond Polymer Refine Detection) and diaminobenzidine. The sections were then counterstained with hematoxylin, dehydrated, cleared, and mounted.

Statistics and reproducibility

Each assay was performed in triplicate and independently repeated at least three times. The results are presented as mean ± standard error of mean (SD). Statistical analyses were performed using GraphPad Prism software (version 4.02; GraphPad Software, San Diego, CA). One-way analysis of variance (ANOVA) followed by t-test was used to compare the results. A difference was considered significant if $P<0.05$. Statistical significance was defined as $P<0.05$ (*), $P<0.01$(**), $P<0.001$(***), and $P<0.0001$(****). To determine P values for all Kaplan-Meier survival curve analyses, we used the log-rank (Mantel-Cox) test (*P=0.0003 P=0.0006, P=0.0061,* and *P=0.0014.*)

Data Availability

Source data for Figures 1b–f, 2d, 2h, 2j, 3g, 4a, 4c, 4g, 5a, 5j, 6b, 6c, 6e, 6h–j, 7b–d, 7f, and Supplementary Figures 1a, 1b, 1e, 1f, 4e–g, 5d, 6c–f, 7a, 7b, 7d–f, 7h, and 7i are provided in Supplementary Table 1. All data supporting the findings of this study are available from the corresponding author on reasonable request.

Supplementary Material

Refer to Web version on PubMed Central for supplementary material.

Acknowledgments

We thank all members of Lou lab for their critical discussion of this work. This work was supported by NIH grants CA203561 and CA224921 to Z.L, and was also supported by ENP-RES20180401–02 to S.B.L.

References

1. Long JS & Ryan KM New frontiers in promoting tumour cell death: targeting apoptosis, necroptosis and autophagy. Oncogene 31, 5045–5060 (2012). [PubMed: 22310284]
2. Su Z, Yang Z, Xu Y, Chen Y & Yu Q Apoptosis, autophagy, necroptosis, and cancer metastasis. Mol Cancer 14, 48 (2015). [PubMed: 25743109]
3. Lalaoui N, Lindqvist LM, Sandow JJ & Ekert PG The molecular relationships between apoptosis, autophagy and necroptosis. Semin Cell Dev Biol 39, 63–69 (2015). [PubMed: 25736836]
4. Radogna F, Dicato M & Diederich M Cancer-type-specific crosstalk between autophagy, necroptosis and apoptosis as a pharmacological target. Biochem Pharmacol 94, 1–11 (2015). [PubMed: 25562745]
5. Tanaka T et al. A novel inflammation-related mouse colon carcinogenesis model induced by azoxymethane and dextran sodium sulfate. Cancer Sci 94, 965–973 (2003). [PubMed: 14611673]
6. Neufert C, Becker C & Neurath MF An inducible mouse model of colon carcinogenesis for the analysis of sporadic and inflammation-driven tumor progression. Nat Protoc 2, 1998–2004 (2007). [PubMed: 17703211]
7. Welz PS et al. FADD prevents RIP3-mediated epithelial cell necrosis and chronic intestinal inflammation. Nature 477, 330–334 (2011). [PubMed: 21804564]
8. Rubin DC, Shaker A & Levin MS Chronic intestinal inflammation: inflammatory bowel disease and colitis-associated colon cancer. Front Immunol 3, 107 (2012). [PubMed: 22586430]
9. Grivennikov SI Inflammation and colorectal cancer: colitis-associated neoplasia. Semin Immunopathol 35, 229–244 (2013). [PubMed: 23161445]
10. Kim ER & Chang DK Colorectal cancer in inflammatory bowel disease: the risk, pathogenesis, prevention and diagnosis. World J Gastroenterol 20, 9872–9881 (2014). [PubMed: 25110418]
11. Pasparakis M & Vandenabeele P Necroptosis and its role in inflammation. Nature 517, 311–320 (2015). [PubMed: 25592536]
12. Seifert L et al. The necrosome promotes pancreatic oncogenesis via CXCL1 and Mincle-induced immune suppression. Nature 532, 245–249 (2016). [PubMed: 27049944]
13. Cho YS et al. Phosphorylation-driven assembly of the RIP1-RIP3 complex regulates programmed necrosis and virus-induced inflammation. Cell 137, 1112–1123 (2009). [PubMed: 19524513]
14. Sun L et al. Mixed lineage kinase domain-like protein mediates necrosis signaling downstream of RIP3 kinase. Cell 148, 213–227 (2012). [PubMed: 22265413]
15. Wu XN et al. Distinct roles of RIP1-RIP3 hetero- and RIP3-RIP3 homo-interaction in mediating necroptosis. Cell Death Differ 21, 1709–1720 (2014). [PubMed: 24902902]
16. Davies SP, Carling D & Hardie DG Tissue distribution of the AMP-activated protein kinase, and lack of activation by cyclic-AMP-dependent protein kinase, studied using a specific and sensitive peptide assay. Eur J Biochem 186, 123–128 (1989). [PubMed: 2574667]

17. Kemp BE et al. AMP-activated protein kinase, super metabolic regulator. Biochem Soc Trans 31, 162–168 (2003).
18. Shimura H et al. Familial Parkinson disease gene product, parkin, is a ubiquitin-protein ligase. Nat Genet 25, 302–305 (2000). [PubMed: 10888878]
19. Yamamoto A et al. Parkin phosphorylation and modulation of its E3 ubiquitin ligase activity. J Biol Chem 280, 3390–3399 (2005). [PubMed: 15557340]
20. Moore DJ, West AB, Dikeman DA, Dawson VL & Dawson TM Parkin mediates the degradation-independent ubiquitination of Hsp70. J Neurochem 105, 1806–1819 (2008). [PubMed: 18248624]
21. Chen D et al. Parkin mono-ubiquitinates Bcl-2 and regulates autophagy. J Biol Chem 285, 38214–38223 (2010). [PubMed: 20889974]
22. Iguchi M et al. Parkin-catalyzed ubiquitin-ester transfer is triggered by PINK1-dependent phosphorylation. J Biol Chem 288, 22019–22032 (2013). [PubMed: 23754282]
23. Kane LA et al. PINK1 phosphorylates ubiquitin to activate Parkin E3 ubiquitin ligase activity. J Cell Biol 205, 143–153 (2014). [PubMed: 24751536]
24. Koyano F et al. Ubiquitin is phosphorylated by PINK1 to activate parkin. Nature 510, 162–166 (2014). [PubMed: 24784582]
25. Picchio MC et al. Alterations of the tumor suppressor gene Parkin in non-small cell lung cancer. Clin Cancer Res 10, 2720–2724 (2004). [PubMed: 15102676]
26. Fujiwara M et al. Parkin as a tumor suppressor gene for hepatocellular carcinoma. Oncogene 27, 6002–6011 (2008). [PubMed: 18574468]
27. Poulogiannis G et al. PARK2 deletions occur frequently in sporadic colorectal cancer and accelerate adenoma development in Apc mutant mice. Proc Natl Acad Sci U S A 107, 15145–15150 (2010). [PubMed: 20696900]
28. Veeriah S et al. Somatic mutations of the Parkinson's disease-associated gene PARK2 in glioblastoma and other human malignancies. Nat Genet 42, 77–82 (2010). [PubMed: 19946270]
29. Lee SB et al. Parkin Regulates Mitosis and Genomic Stability through Cdc20/Cdh1. Mol Cell 60, 21–34 (2015). [PubMed: 26387737]
30. Lee S et al. Multiple-level validation identifies PARK2 in the development of lung cancer and chronic obstructive pulmonary disease. Oncotarget 7, 44211–44223 (2016). [PubMed: 27329585]
31. Thomas M Inflammation in Parkinson's disease. (Springer, New York; 2014).
32. Noble CL et al. Regional variation in gene expression in the healthy colon is dysregulated in ulcerative colitis. Gut 57, 1398–1405 (2008). [PubMed: 18523026]
33. Li J et al. The RIP1/RIP3 necrosome forms a functional amyloid signaling complex required for programmed necrosis. Cell 150, 339–350 (2012). [PubMed: 22817896]
34. Deng M et al. Deubiquitination and Activation of AMPK by USP10. Mol Cell 61, 614–624 (2016). [PubMed: 26876938]
35. Gonzalez-Juarbe N et al. Pore-Forming Toxins Induce Macrophage Necroptosis during Acute Bacterial Pneumonia. PLoS Pathog 11, e1005337 (2015). [PubMed: 26659062]
36. Wagener C, Stocking C & Müller O Cancer Signaling: From Molecular Biology to Targeted Therapy. (Wiley-Blackwell, 2016).
37. Gwinn DM et al. AMPK phosphorylation of raptor mediates a metabolic checkpoint. Mol Cell 30, 214–226 (2008). [PubMed: 18439900]
38. Canto C et al. AMPK regulates energy expenditure by modulating NAD+ metabolism and SIRT1 activity. Nature 458, 1056–1060 (2009). [PubMed: 19262508]
39. Mandal P et al. RIP3 induces apoptosis independent of pronecrotic kinase activity. Mol Cell 56, 481–495 (2014). [PubMed: 25459880]
40. Yang XS et al. Hypoxia-inducible factor-1 alpha is involved in RIP-induced necroptosis caused by in vitro and in vivo ischemic brain injury. Sci Rep 7, 5818 (2017). [PubMed: 28724891]
41. Los M et al. Activation and caspase-mediated inhibition of PARP: a molecular switch between fibroblast necrosis and apoptosis in death receptor signaling. Mol Biol Cell 13, 978–988 (2002). [PubMed: 11907276]
42. Eguchi Y, Shimizu S & Tsujimoto Y Intracellular ATP levels determine cell death fate by apoptosis or necrosis. Cancer Res 57, 1835–1840 (1997). [PubMed: 9157970]

43. Tsujimoto Y Apoptosis and necrosis: intracellular ATP level as a determinant for cell death modes. Cell Death Differ 4, 429–434 (1997). [PubMed: 16465263]

44. Nikoletopoulou V, Markaki M, Palikaras K & Tavernarakis N Crosstalk between apoptosis, necrosis and autophagy. Biochim Biophys Acta 1833, 3448–3459 (2013). [PubMed: 23770045]

45. Rothfuss O et al. Parkin protects mitochondrial genome integrity and supports mitochondrial DNA repair. Hum Mol Genet 18, 3832–3850 (2009). [PubMed: 19617636]

46. Omoto S et al. Suppression of RIPK3-dependent necroptosis by human cytomegalovirus. J Biol Chem 290, 11635–11648 (2015). [PubMed: 25778401]

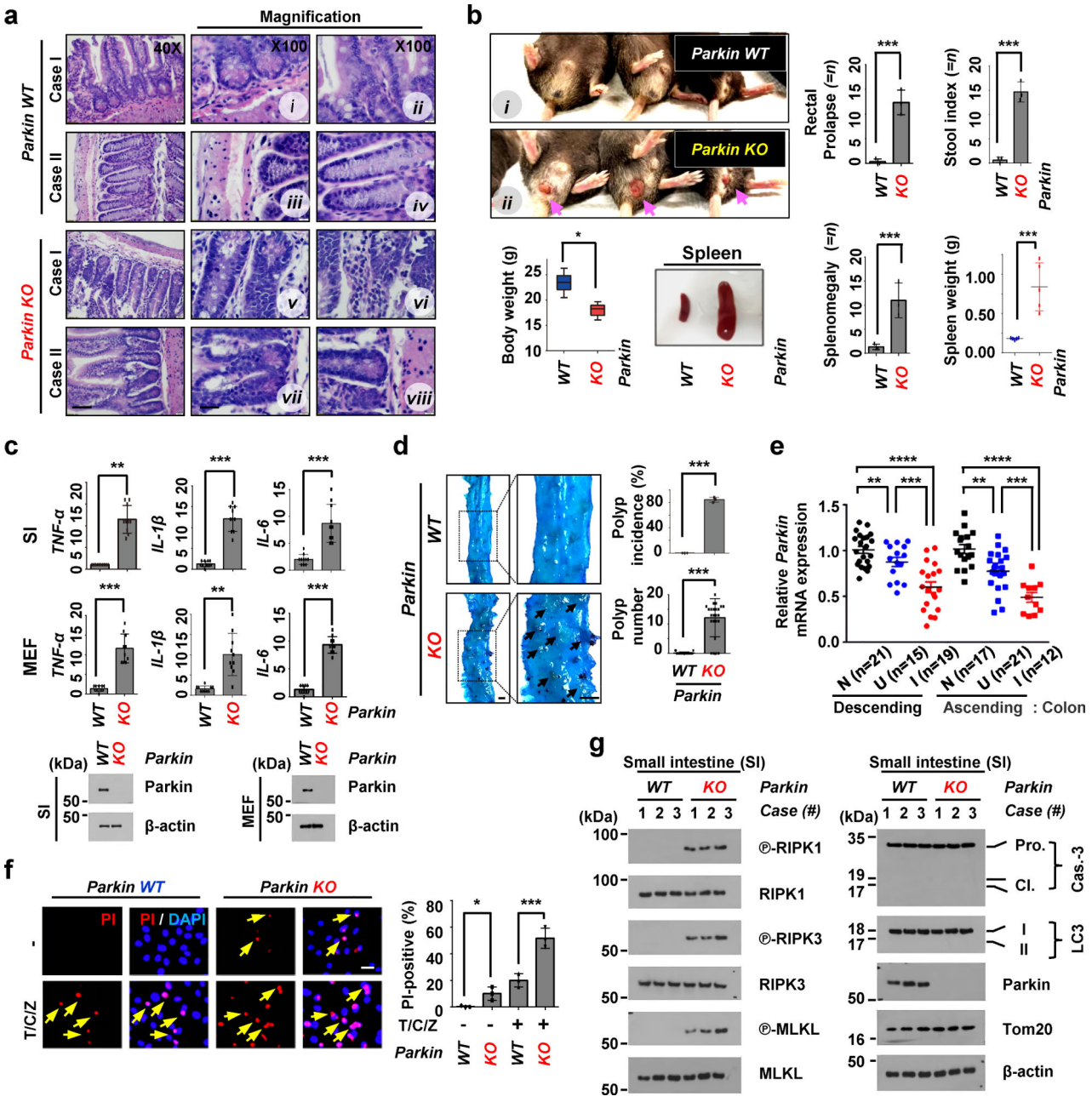

Fig. 1. *Parkin* knockout (*KO*) mice have increased inflammation and spontaneous tumor formation.

a-b, *Parkin WT* and *KO* mice at 10 months of age were analyzed for inflammation by Immunohistochemistry (*n* = 20 mice, small intestine (SI) tissues, a) or body weight (n=25 mice), the incidence of rectal prolapse (RP, Pink arrows), stool index (blood content in the stool), splenomegaly (*n* = 25 mice, three independent experiments) or weight of spleen (*n* = 5 mice) (b). Representative images from *Parkin WT* and *KO* mice (case I and case II, 40×; i-viii, magnification, 100×). *Parkin WT* (i) and *KO* (ii) mice at 10 months of age (b). **c,** *mRNA* levels of the cytokines, *TNF-α, IL-1β, and IL-6* were assessed in the small intestine of *Parkin WT* and *KO* mice and MEFs (*n = 10*). Tissue (SI) or MEFs lysates were subjected

to immunoblot as indicated (*bottom*). **d,** Representative images of polyps in the small intestine of *Parkin WT* and *KO* mice at 12 months. Polyp number was determined in the proximal, middle and distal intestine in mice. Arrows, large adenomatous polyps (adenomas). $n = 25$. **e,** Gene expression of *Parkin* in human ulcerative colitis (colon) tissues. Gene expression omnibus data sets GE11223. N, Normal; U, Uninflamed; I, Inflamed. **f,** *Parkin WT* and *KO* MEFs were treated with necrotic stimulation, T/C/Z; TNF-α (20 ng/mL), CHX (10 μg/mL) and z-VAD (20 μM) for 4 h and stained with propidium iodide (PI). Arrows; necroptosis. 100 cells were monitored in each experiment. **g,** The small intestine tissues of *Parkin WT* and *KO* mice (n=3 mice/genotype) at 10 months of age were lysed, and tissues lysates were blotted with the indicated antibodies. Pro., pro-caspase; Cl., cleavage; Cas.−3, caspase-3. Data in c,e are represented as the mean ±s.e.m. Data in b,d,f are represented as the mean ±s.e.m. of three independent experiments. Statistical analysis was performed by one-way ANOVA (PRISM software). **P<0.05*, ***P<0.01*, ****P<0.001, ****P<0.0001*; *n.s.*, not significant. Statistic source data (b,c,d,e,f) are provided in Supplementary Table 1 and unprocessed blots (c, g) are provided in Supplementary Figure 8, respectively. Scale bars, 200 μm (a), and 1 cm (d) and 20 μm (f).

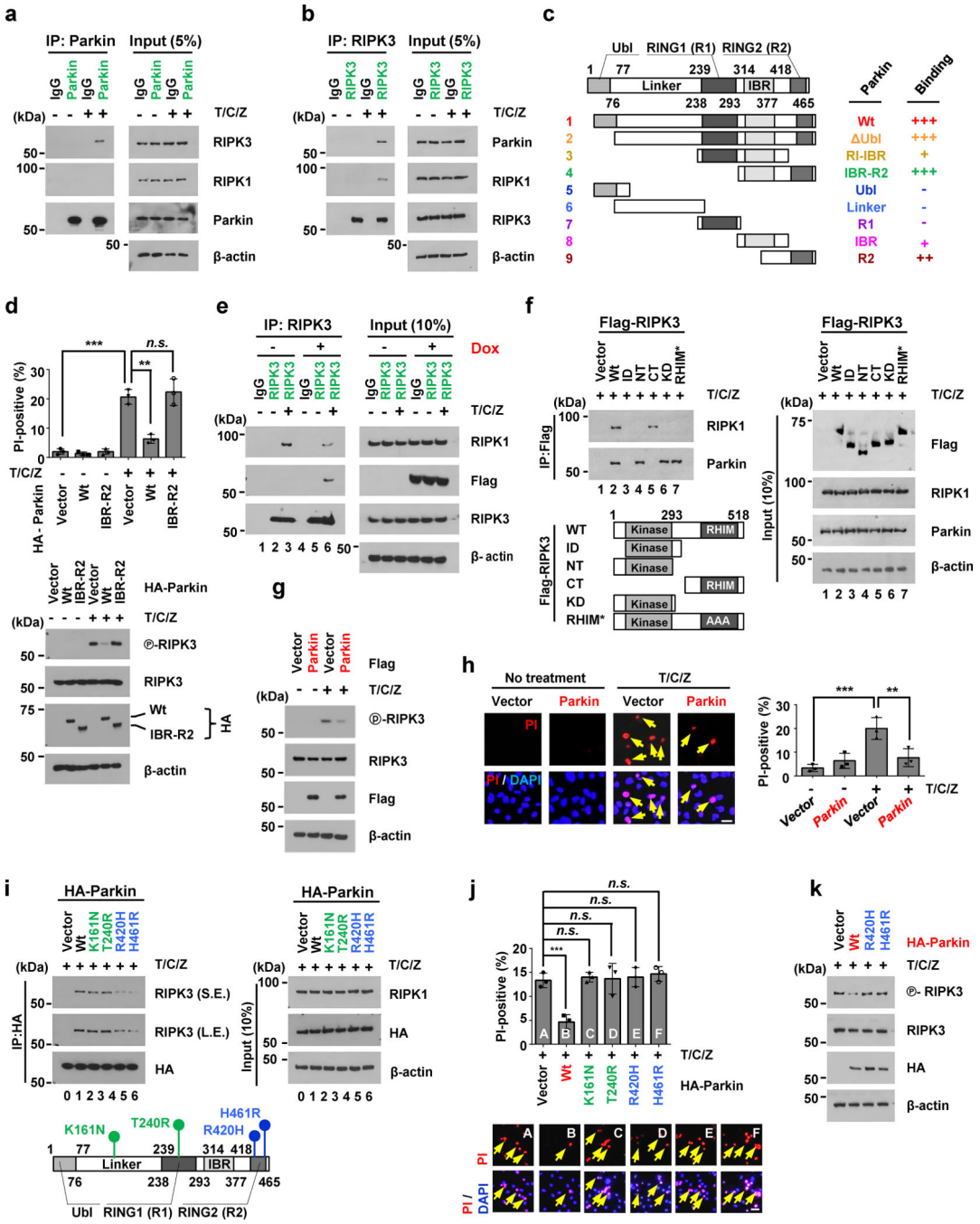

Fig. 2. Parkin negatively regulates the RIPK1-RIPK3 interaction.

a-b, HT-29 cells were treated with T/C/Z for 4h. Cell lysates were then subjected to IP and immunoblotted as indicated. **c,** Schematic diagram of Parkin structure. + and - symbols, the binding affinity of each deletion mutant with RIPK3 is indicated. **d,** Cells were transfected with the indicated constructs and then treated with T/C/Z for 4 h. Cell were subjected to PI staining (*top*) or subjected to immunoblot with the indicated antibodies (*bottom*). **e,** *Parkin* KO MEFs transfected with the epitope-tagged doxycycline-inducible expression vector were induced to express Parkin, and the Parkin-RIPK3 interaction was examined by co-

immunoprecipitation. Dox., doxycycline. **f,** Cells were transfected with the indicated plasmids and collected for immunoprecipitation (IP) and immunoblot analysis. Schematic diagram of RIPK3 domain structure. RHIM*, a mutant (Mut) RIPK3 (alanine cluster disruption of RHIM). **g-h,** cell were transfected with the indicated constructs and then treated with T/C/Z for 4 h. Cell lysates were subjected to immunoblot with the indicated antibodies (g) or subjected to PI staining (h) shown are representative images for each stain (*top*) and quantification of PI-positive cells (*bottom*). PI-positivity or yellow arrows indicates necroptosis. 100 cells were monitored in each experiment (h). **i,** Cells were transfected with the indicated constructs (WT, R420H, or H461R) and then treated with T/C/Z for 4 h. Cell lysates were then subjected to IP and immunoblotted as indicated (h, *top*). Schematic diagram of Parkin structure (h, *bottom*). **j-k,** Cells were transfected with the indicated constructs and then treated with T/C/Z for 4 h. For necroptosis, cells were stained with PI (j), and cell lysates were blotted with the indicated antibodies (k). Quantification of PI-positive cells (j, *top*) and representative images for each stain (j, *bottom*). PI-positive (arrows): necroptosis. (j). Data in d,h,j are represented as the mean ±s.e.m. of $n=3$ independent experiments. Statistical analysis was performed by one-way ANOVA (PRISM software). $*P<0.05$, $**P<0.01$, $***P<0.001$; *n.s.*, not significant. Statistic source data (d,h,j) are provided in Supplementary Table 1 and unprocessed blots (a,b,d,e,f,g,i,k) are provided in and Supplementary Figure 8, respectively. Scale bars, 20 μm (h,j).

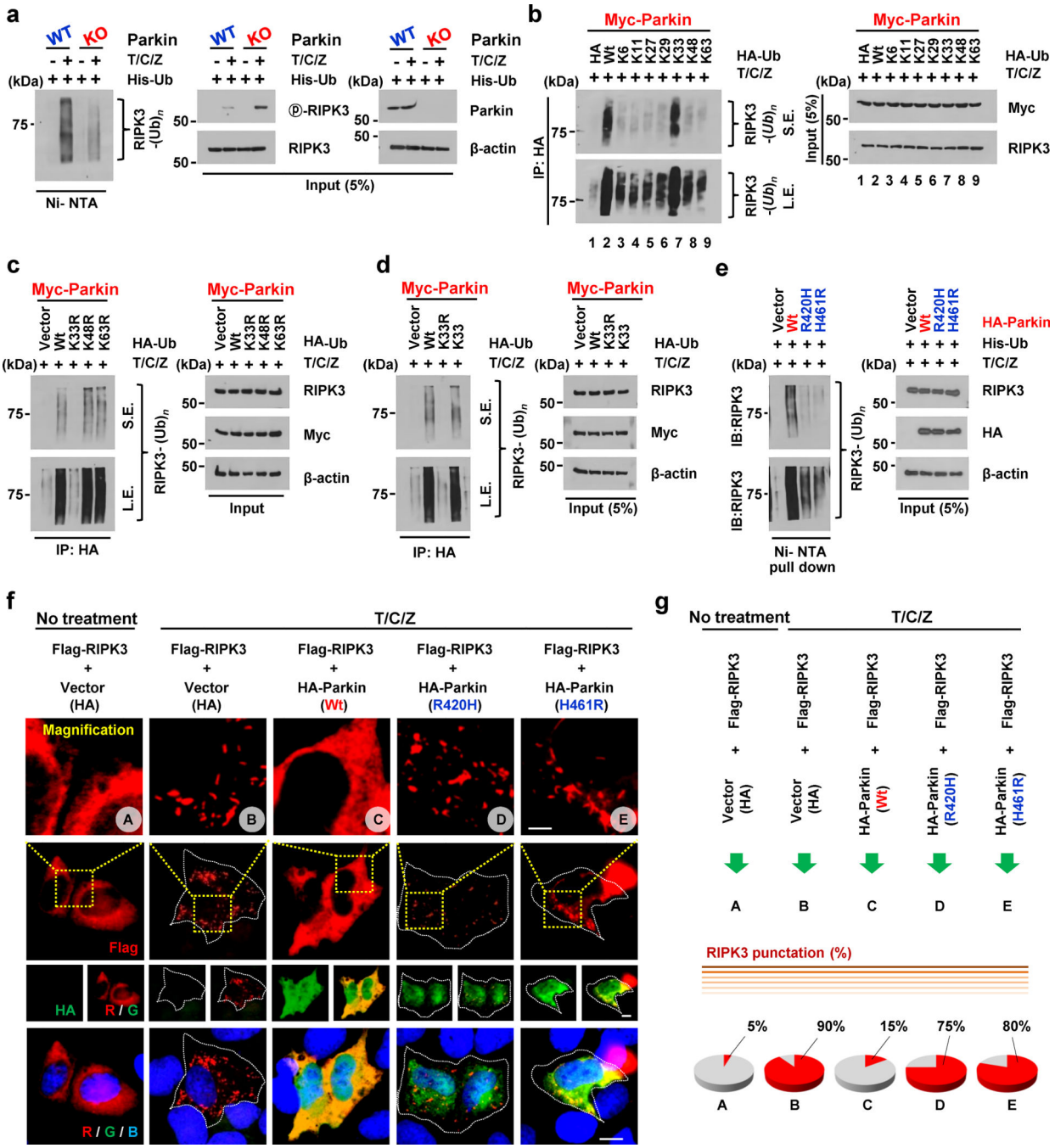

Fig. 3. Parkin promotes K33-linked polyubiquitination of RIPK3.

a, *Parkin WT* and *KO* MEFs were treated with T/C/Z for 4 h. Ubiquitinated proteins were pull down under denaturing conditions by Ni-NTA agarose and analyzed by immunoblot. **b**, Cells were transfected with the indicated plasmids (Ubiquitin: WT, K6, K11, K27, K29, K33, K48, or K63 only) and then treated with T/C/Z for 4 h. Cell lysates were then subjected to IP and immunoblotted as indicated. SE, short exposure; LE, long exposure. **c-d,** Cells were transfected with the indicated plasmids (Ubiquitin: WT, K33R, K48R, K63R, or K33 only) and then treated with T/C/Z for 4 h. Cell lysates were then subjected to IP and

immunoblotted as indicated. SE, short exposure; LE, long exposure. **e,** Cells were transfected with the indicated constructs (Parkin WT, R420H, or H461R) and then treated with T/C/Z. Ubiquitinated proteins were pulled down under denaturing conditions by Ni-NTA agarose and analyzed by immunoblot. **f-g,** U2OS cells were transfected with the indicated constructs and then treated with T/C/Z for 4 h. The distribution of RIPK3 (Red) was detected using immunofluorescence (f). Quantification of RIPK3 punctation (g). Scale bar, 20 μm (magnification, 200 μm). All experiments were repeated independently at least three times with similar results. Source data are provided in Supplementary Table 1. Uncropped images of blots for (a,b,c,d,e) are shown in Supplementary Figure 8. Scale bars, 20 μm (magnification, 200 μm, f).

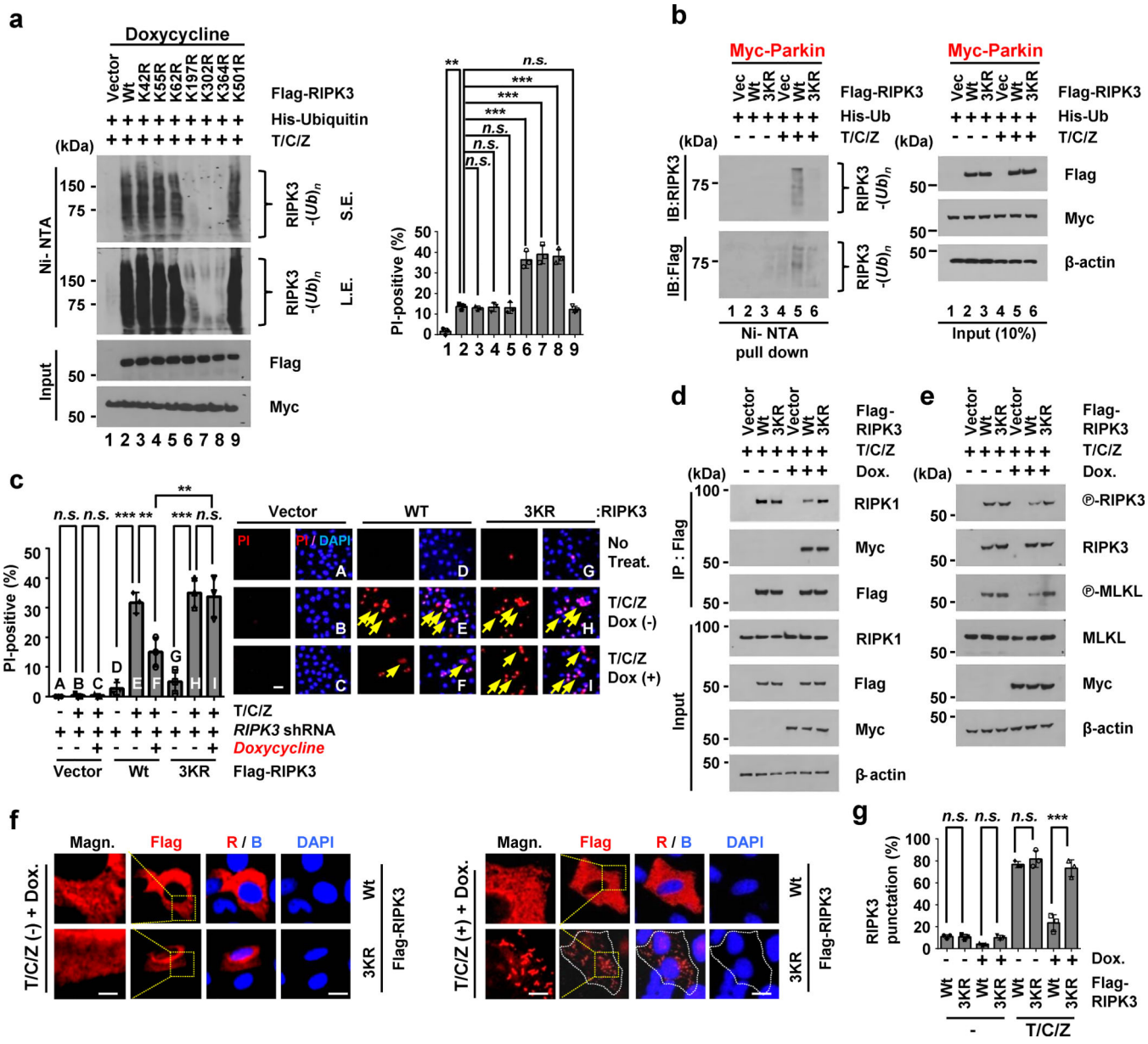

Fig. 4. The Parkin-mediated RIPK3 ubiquitination is important for RIPK3 inhibition.

a, HT-29 cells depleted of RIPK3 were transfected with the indicated constructs (vector, RIPK3 WT, K42R, K55R, K62R, K197R, K302R, K364R, or K501R) and then treated with doxycycline to induce Parkin expression and T/C/Z. Ubiquitinated proteins were pulled down under denaturing conditions by Ni-NTA agarose and analyzed by immunoblotting (*left*). Cells were analyzed by PI staining (*right*). Quantification of PI-positive cells. 100 cells were monitored in each experiment. **b-c,** HT-29 cells depleted of *RIPK3* were transfected with the indicated constructs (RIPK3 WT or 3KR) and then treated doxycycline to induce Parkin expression and T/C/Z. Ubiquitinated proteins were pulled down under denaturing conditions by Ni-NTA agarose and analyzed by immunoblot (b). Cell death was analyzed by PI staining (c). Quantification of PI positive cells (*left*) and representative images for each condition (*right*). 100 cells were monitored in each experiment. Dox.,

doxycycline. Arrows indicate necroptosis. **d-e,** HT-29 cells depleted of RIPK3 were transfected with the indicated constructs (vector, RIPK3 WT, or 3KR) and then treated doxycycline and T/C/Z. Cell lysates were then subjected to IP and immunoblotted as indicated. Dox., doxycycline. **f-g,** Cells as (d) were treated with T/C/Z for 4 h and the distribution of RIPK3 (Red) was detected using immunofluorescence (f). Quantification of RIPK3 punctuation (g). 100 cells were monitored in each experiment. Data in a,c,g are represented as the mean ±s.e.m. of *n=3* independent experiments. Statistical analysis was performed by one-way ANOVA (PRISM software). ***P<0.01*, ****P<0.001*; *n.s.*, not significant. Statistic source data (a,c,g) are provided in Supplementary Table 1 and unprocessed blots (b,d,e) are provided in Supplementary Figure 8, respectively. Scale bars, 20 μm (c,f).

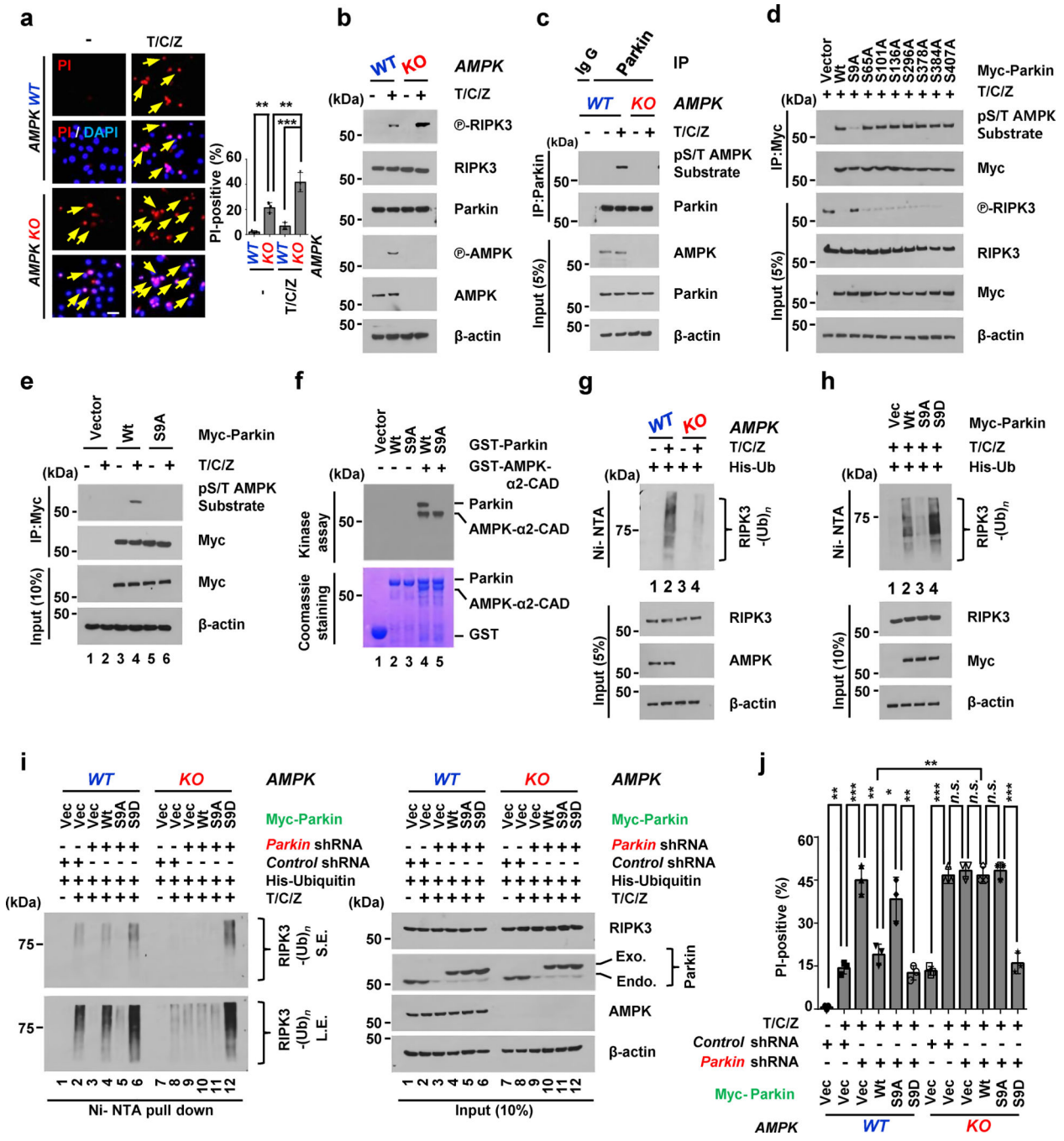

Fig. 5. Parkin is activated by AMPK-dependent phosphorylation at Ser 9 (S9) during necroptosis.

a-b, *AMPK WT* and *KO* MEFs were treated with T/C/Z for 4 h. Cells were then stained with PI (a), or cell lysates were analyzed by immunoblotting with the indicated antibodies (b). Shown are representative images of cells under each condition (a, *left*) and quantification of PI-positive cells (a, *right*). 100 cells were monitored in each experiment. Arrows: necroptosis. **c,** *AMPK WT,* and *KO* MEFs were treated with necrotic stimulation for 4 h, and cell lysates were then subjected to IP and immunoblotted as indicated. **d-e,**

Parkin KO MEFs were transfected with the indicated constructs (Parkin WT, S9A, S65A, S101A, S136A, S296A, S378A, S384A, or S407A) and then treated with necrotic stimulation. Cell lysates were then subjected to IP and immunoblotted as indicated. **f,** Constitutively active GST-AMPK kinase domain (GST-AMPK-CAD (T172D)) was incubated with wild-type or the S9A mutant of GST-Parkin in *in vitro* kinase assay. The autoradiograph and the Coomassie blue staining of protein bands are shown. **g,** *AMPK WT,* and *KO* MEFs were treated by T/C/Z for 4 h. Ubiquitinated proteins were pulled down under denaturing conditions by Ni-NTA agarose and analyzed by immunoblotting with the indicated antibodies. **h**, Cells were transfected with the indicated constructs (WT, S9A, or S9D) and then treated with necrotic stimulation. RIPK3 ubiquitination was then examined as before. **i-j,** *AMPK WT* and *KO* MEFs were transfected with the indicated constructs (*Control* shRNA, *Parkin* shRNA, Parkin WT, S9A, or S9D) and then treated with necrotic stimulation for 4 h. RIPK3 ubiquitination (i) and necroptosis (j) were then examined as before. SE, short exposure; LE, long exposure; Exo, exogenous; Endo, endogenous. Quantification of PI-positive cells under each condition. 100 cells were monitored in each experiment. Dox., doxycycline; Vec., vector. Data in a,j are represented as the mean ±s.e.m. of *n=3* independent experiments. Statistical analysis was performed by one-way ANOVA (PRISM software). **P<0.05*, ***P<0.01*, ****P<0.001*; *n.s.*, not significant. Statistic source data (a,j) are provided in Supplementary Table 1 and unprocessed blots (b,c,d,e,f,g,h,i) are provided in Supplementary Figure 8, respectively. Scale bars, 20 μm (a).

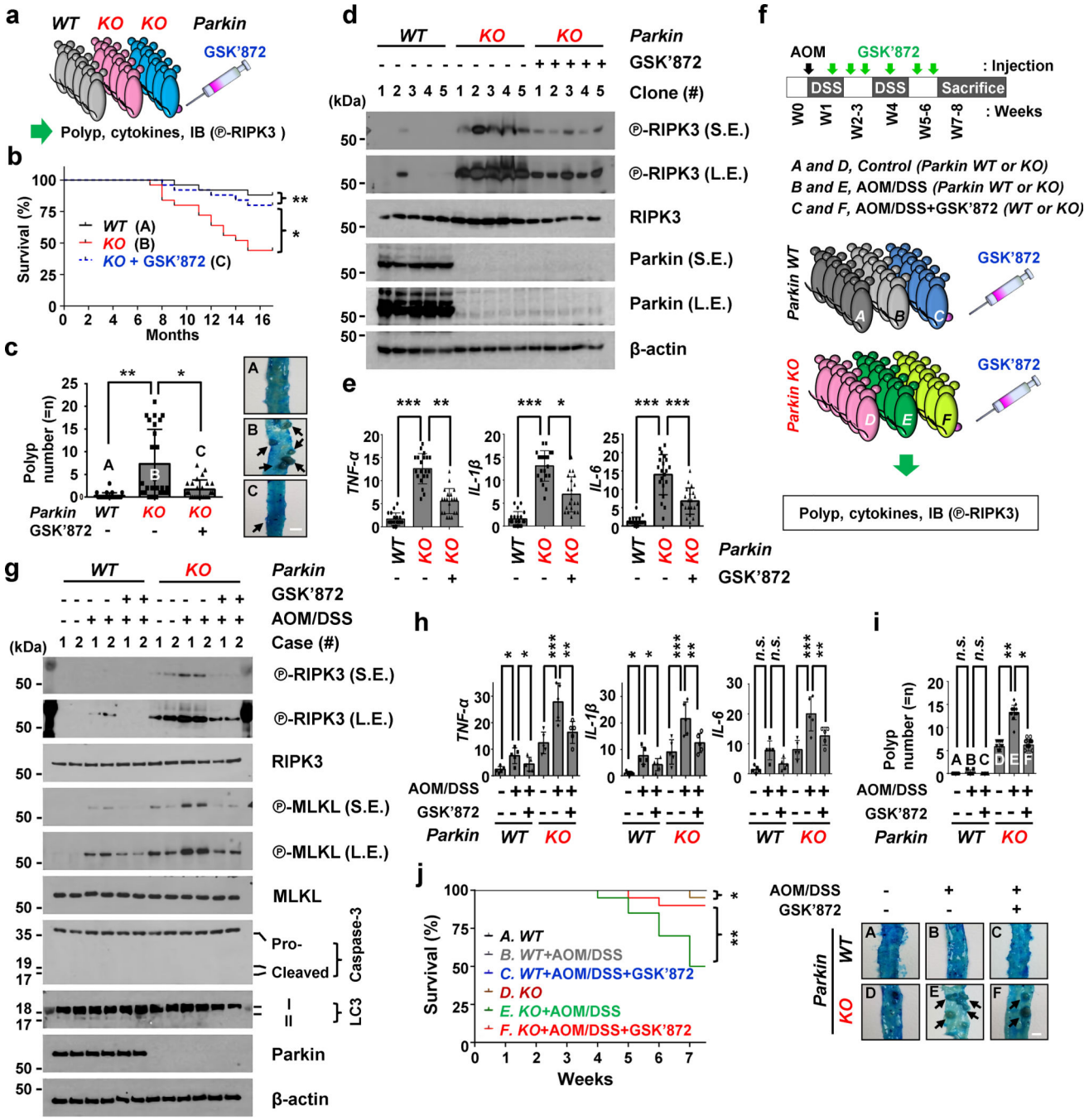

Fig. 6. RIPK3 inhibition suppresses intestinal inflammation and colitis-associated tumorigenesis in AOM/DSS mouse model.

a-e, *Parkin WT* and *KO* mice (*n=25 mice;* 10 mice for histological analysis, 15 mice for protein expression analysis) at 2 months of age were intravenously (i.v.) treated with either the vehicle control or GSK'872 at a dose of 1.0 mg/kg once weekly. The schematic model for experimental animal design (a), % survival (months, b), representative images and number of polyps (c, *n=25 mice*), expression of the indicated proteins (d), and mRNA levels of inflammatory cytokines (*TNF-α, IL-1β, or IL-6, n=20 mice,* e) are shown. Arrows: large

adenomatous polyps (adenomas, c). SE, short exposure; LE, long exposure. **f-j,** *Parkin WT* and *KO* mice (*n=20 mice/genotype/treatment*) were treated to establish an AOM/DSS model of colitis-associated colon cancer (CAC). These mice were treated i.v. with either the vehicle control or GSK'872 at a dose of 1.0 mg/kg twice weekly. The schematic model (f), expression of the indicated proteins (g), mRNA levels of the indicated cytokines (*TNF-α, IL-1β, or IL-6*, *n=5 mice,* h), number of polyps (*n=25 mice*, i, *top*) and representative images (*n=25 mice*, i, *bottom*) and % survival (j) are shown. Arrows indicate large adenomatous polyps (adenomas, i). SE, short exposure; LE, long exposure. Pro., pro-caspase; Cl., cleavage; Cas.−3, caspase-3. Data in b,c,e,h,I,j are represented as the mean ±s.e.m. of *n=3* independent experiments. Statistical analysis was performed by one-way ANOVA (PRISM software). **P<0.05*, ***P<0.01*, ****P<0.001*; *n.s.*, not significant. Statistic source data (b,c,e,h,I,j) are provided in Supplementary Table 1 and unprocessed blots (d,g) are provided in Supplementary Figure 8, respectively.

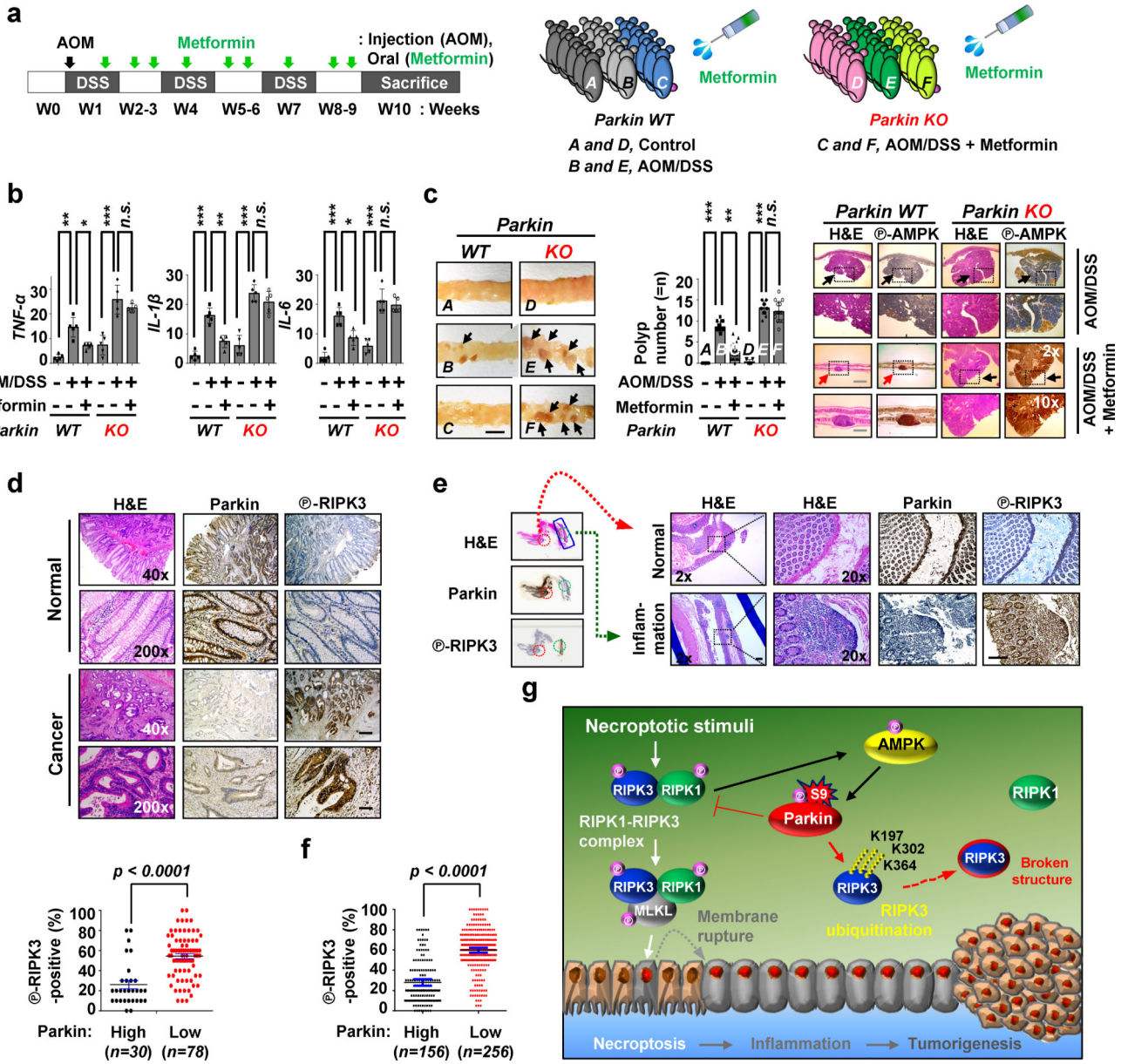

Fig. 7. AMPK activation inhibits colitis-associated cancer in a *Parkin*-dependent manner.

a-c, *Parkin WT* and *KO* mice were treated to establish an AOM/DSS model of colitis-associated colon cancer (CAC). Mice were fed with metformin (300 mg/kg) for 10 weeks. The schematic model (a), mRNA levels of the indicated cytokines (b, *n=5 mice/group*), and Representative images and quantification of a number of polyps under the indicated treatment conditions (c, *n=15 mice/group*) are shown. Arrows indicate large adenomatous polyps (adenomas, c, *left*). The results shown are the mean number of polyps/mouse ± s.d (c, *middle*). Immunohistochemistry showing AMPK activation (c, *right*). **d,** Immunohistochemistry showing reciprocal expression of Parkin and phospho-RIPK3 protein in human colon cancer tissues compared with normal. Serial tumor sections from the same patient were processed. Scale bar, 50 μm. 40×, 100× (*left*). Quantification of the expression of Parkin/ phospho-RIPK3 in human colon cancer tissues is shown (*below*). **e-f,**

Immunohistochemistry showing reciprocal expression of Parkin and phospho-RIPK3 protein in human tissues from patients with inflammatory bowel disease (IBD, Crohn's disease or Ulcerative colitis) compared with normal. Representative microscopy images of Parkin and phospho-RIPK3 expression Serial tissue sections from the same patient were processed. Quantification of the expression of Parkin/ phospho-RIPK3 in human inflammation tissues is shown (f). **g,** A Schematic model of how the AMPK-Parkin axis negatively regulates necroptosis and tumorigenesis via RIPK3 inhibition. Data in b,c,d,e,f are represented as the mean ±s.e.m. Statistical analysis was performed by one-way ANOVA (PRISM software). **P<0.05*, ***P<0.01*, ****P<0.001*; *n.s.*, not significant. Statistic source data for b,c,d,f are provided in Supplementary Table 1. Scale bars, 50 μm (c,d,e) and 1 cm (c).